Shock Detection from Computational Fluid Dynamics Results

David Lovely*
Massachussetts Institute of Technology, Cambridge, MA 02139

Robert Haimes†
Massachussetts Institute of Technology, Cambridge, MA 02139

In complex flow regimes, it may be difficult for an analyst to find the location of shock discontinuities within a Computational Fluid Dynamics (CFD) solution. They do not correspond to locations where the mach number is unity, and the high gradients associated with the discontinuity can be difficult to detect because of numerical smoothing performed in order to obtain the solution. An algorithm is introduced that uses the flow physics to locate shocks in transient and steady state solutions. The test was validated with simple one and two dimensional models, then extended to more realistic three dimensional flows. A set of filtering algorithms was developed to remove any false shock indications. Results indicate that both the stationary and transient shock finding algorithms accurately locate shocks, but need filtering to compensate for a lack of sharpness in CFD discontinuities.

Nomenclature

P	Pressure
ρ	Density
a	Speed of sound
$U = \|\vec{q}\|$	Speed
M	Mach number
$\vec{M} = \frac{\vec{q}M}{U}$	Mach vector
γ	ratio of specific heats
$\vec{q}$	Velocity

Introduction

Shock waves are a type of compression wave in flow fields that may occur when the velocity of the fluid exceeds the local speed of sound. The state of the fluid as described by the pressure, velocity and other primitive variables can change radically across a shock boundary that is approximately the thickness of one over the Reynolds number, making them almost discontinuities in typical flows of high Reynolds number. These discontinuites are of interest to designers because their strength and location affects the drag on aircraft, the functioning of inlets, the efficiency of nozzles and a host of other design problems in fluid mechanics.

The shock location problem is analogous to finding edges in an image, the purpose of both applications is to find discontinuities in a scalar field that contain large spacial variations in the scalar along with noise and smoothing. In the case of CFD solutions, the noise in the solution is analogous to dispersion and the smoothing is related to dissipation. Figure 1 shows how pressure through a real shock differs from a numerically simulated shock. Dissipation blurs the edges of the shock, making it hard to determine it's extent. Dispersion creates the high frequency noise on the edges of the shock.

There are two basic approaches to detecting shock discontinuites. The first approach is to view it as an edge detection problem and apply the methods that have been developed in that field. Alternatively, the physics of shocks can be used to create a detection algorithm that is not applicable to the more general problem. This paper takes the physical approach since there is not a generally agreed on 'best' edge detection algorithm and by looking at the physics, it might be possible to formulate a more rigorous detector.

In the past, shock waves have been extracted with an edge detection technique which has been described by Ma, Rosendale, and Vermeer.[1] This technique searches for inflection points in the pressure or density fields by finding areas where the laplacian of the scalar quantity goes to zero. This works because some scalar quantities like pressure and density monotonically and smoothly increase through the shock, requiring the second derivative of the scalar to go through zero in the shock. However, this detector will pick up other features that are not shocks. There can be expansion waves in a flow solution that are similar to shock features, but pressure and density decrease along streamlines through the expansion. The second derivatives of pressure and density are also zero in quiescent flow like regions far from a body. Both these features have to be removed from the marked areas. One advantage of this approach is that it also captures moving shocks in a transient solution, since pressure and density are invariant quantities, unchanged when

*Graduate Student
†Principal Research Engineer

the frame of reference is attached to a moving shock.

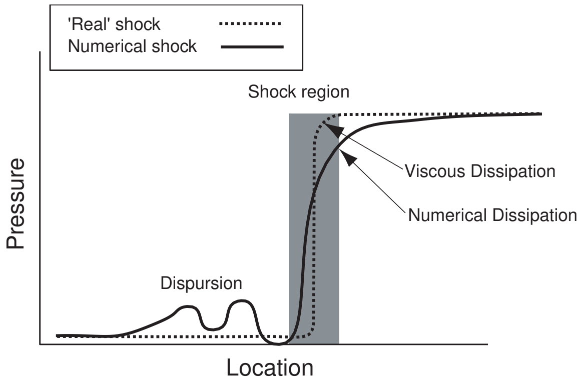

Fig. 1 Shock inflection points

The second method is the one advocated in this paper, which is to use the pressure gradient to find the value of the mach number normal to a shock. The approach was outlined by David Darmofal[3] and also implemented in Plot3D.[5] Since the shock surface normal will be aligned with the pressure gradient vector, the mach number in the direction of this vector is the normal mach number. A shock is then located where this normal mach number is greater than or equal to unity.

One disadvantage of this shock finding method is that it will fail to capture some moving shocks in transient solutions. The mach vector is calculated in the CFD solution relative to the model frame of reference. But the shock calculation needs the mach vector in the shock frame of reference. For example, a shock traveling in a shock tube can exist when the fluid in the tube is moving at a velocity less than the speed of sound. Only when the mach number is calculated with respect to the moving shock would this shock be detected. Correction terms can be added to the basic equation to compensate for the change in reference frame and make the detector valid for moving shocks.

Shock Visualization

Shock waves in high Reynolds number flows have a thickness on the order of a few molecular mean free paths, so they can be visualized as surfaces in a three dimensional flow. In moving to a three dimensional numerical model, the previous work by Ma, Rosendale, and Vermeer[1] has tried to preserve the surface representation. Similar work by Pagendarm and Seiz[4] refers to shocks as "invisible surfaces" that should be made visible by computer rendering. But, because of the descritization and numerical effects of modeling such sharp discontinuities, the shock location is actually spread out into a three dimensional region of space, not just a surface. Even in areas of strong shocks and highly refined grids, this region often looks like a slice of the model volume, with two close and almost parallel surfaces enclosing the shock. Both Pagendarm and Ma, Rosendale[1,4] try to resolve this problem by applying a threshold to the pressure or density gradient magnitude to filter out one of the surfaces. Hesselink, Levy, and Batra[6] take an alternative approach to filtering. They reject all the triangles in the shock surface that have normals that are not aligned with the pressure gradient. Filtering out one surface is not always desirable since the thickness and shape of the region conveys information about the model, the solution, and how well the shock has been detected. Elements marked in the shock region can also be used in a mesh refinement procedure. The only way to collapse the shock region into a surface is to replace the computed variation of temperature density and velocity in this region with a sharp step function that does not violate the mass and momentum conservation principles. However this is not practical since the detected region does not correspond to the actual extent of the shock, making it difficult to find the jump in density, temperature and pressure across the shock. Even though physical shocks can be thought of as surfaces, shocks in numerical models are regions in space.

Stationary Shocks

The stationary shock algorithm was developed with a knowledge of the shock geometry shown in figure 2.

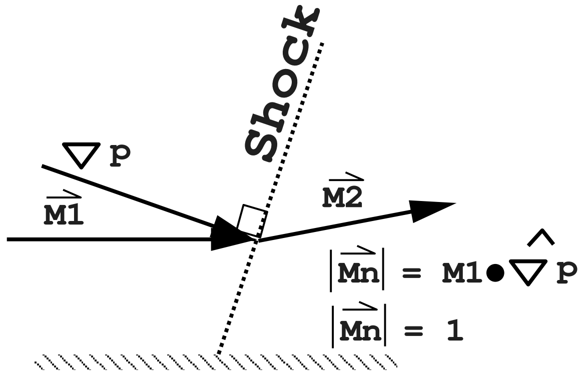

Fig. 2 Shock detection test quantity

For any shock, the mach number normal to the shock has a value of at least one just before the shock. This normal mach number can be approximated on each node and used as a test value for determining the shock location. The pressure gradient is always normal to the shock, so it was used to find the shock orientation. The pressure gradient was approximated for each node, and then dotted with the mach vector to calculate a shock test value at each node. The locations where the test value equals one forms a boundary surrounding the shock location.

This test excludes areas of expansion, since the pressure gradient and the mach vector will have opposite senses, and their dot product will be less than zero.

For three dimensional models, an iso-surface of $M_n = 1$ was used to visualize the results. The shock feature is surrounded by the $M_n = 1$ iso-surface, and has a thickness associated with it. In the two dimensional case, contours of the normal mach number were created, and the $M_n = 1$ curve forms a boundary for a shock region.

Grid Study

A supersonic ramp test case show in figure 3 was constructed to validate the test. The shaded area is the region of the model that was used to plot the results and grids.

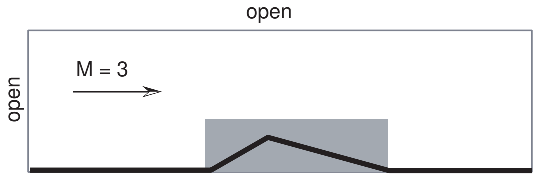

Fig. 3 Ramp model

Three different uniform grids were generated for the same geometry to determine the sensitivity of the detector to grid size. Figure 4 shows the grids that were used for the experiment.

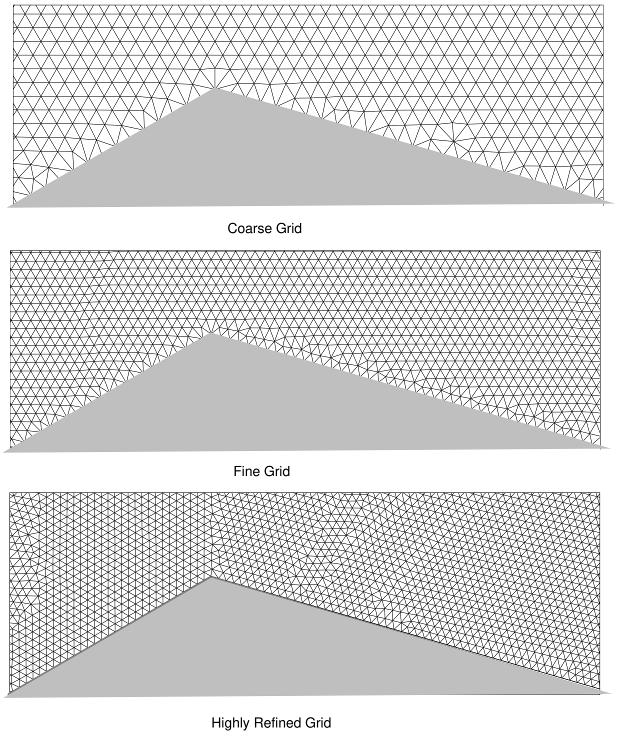

Fig. 4 Triangulation of wedge model

The results of the three runs were similar except for the thickness of the indicated shock. The larger the element size, the larger the indicated shock. Figures 5, 6 and 7 are contour plots of the normal mach number, starting at $M_n = 1$ in the region of the wedge.

The results in table 1 show that the shock algorithm displays shock thickness as a linear function of element size. The shape of the shock region not only locates the shock, but can point to a lack of mesh refinement in the area.

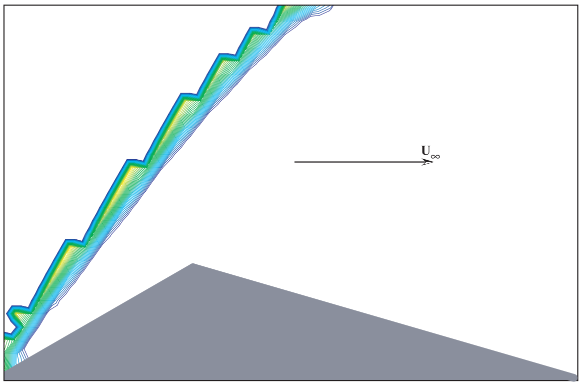

Fig. 5 Shock contours on the coarse grid

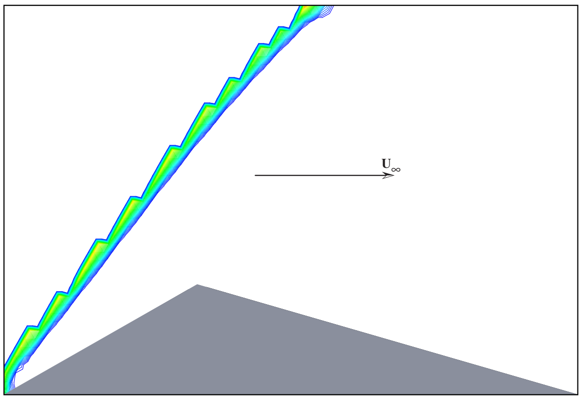

Fig. 6 Shock contours on more refined grid

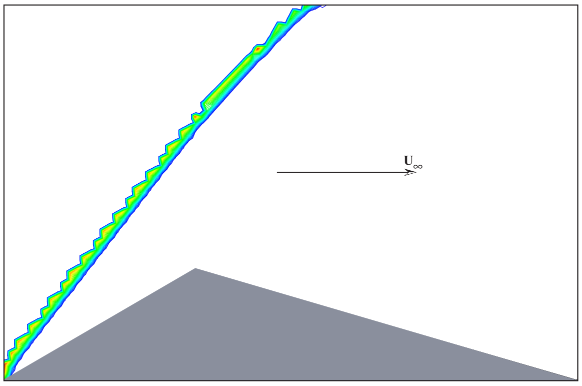

Fig. 7 Shock contours on highly refined grid

Number of elements	Shock thickness (num cells)
5272	3
13801	3
20942	3

Table 1 Grid study results

The numerical model used to solve the problem also greatly effects the shape of the shocks. Some CFD solution algorithms are better suited to capturing the sharp discontinuities. The larger the effective dissipation, the more spread out the shock and the more cells involved.

Transient Modifications

The assumptions made in constructing the previously described shock finding technique no longer apply when the shock is moving. To locate a shock with the previous method, it is necessary to assume that the observer is traveling with the shock and all velocities are measured with respect to this translating frame of reference. However, since all velocities are calculated in the model frame, there has to be a correction applied to the test equation to account for the moving shock. The equation 1 shows what this term must be, basically a time derivative of the pressure.

$$\frac{1}{|\bigtriangledown P|}\frac{1}{a}\frac{Dp}{Dt} = \frac{1}{|\bigtriangledown P|}\frac{1}{a}\frac{dp}{dt} + \frac{\vec{M}\cdot\bigtriangledown P}{|\bigtriangledown P|} \qquad (1)$$

It is more computationally expensive to approximate time derivatives directly, since that would require the storage of multiple time steps. So, the time derivative of pressure was calculated based on relations that equate it to a spacial variation of the state variables. Equation 2 applies to isentropic flows.

$$dp = a^2 d\rho \qquad (2)$$

This equation is then used along with the conservation of mass equation to produce an equation for an invariant test quantity that can be used to locate moving shocks.

$$\frac{dp}{dt} = -a^2 \bigtriangledown\cdot(\rho\vec{q}) \qquad (3)$$

From equations 2 and 3, equation 1 becomes:

$$\frac{1}{|\bigtriangledown P|}\frac{1}{a}\frac{Dp}{Dt} = -a\frac{1}{|\bigtriangledown P|}\bigtriangledown\cdot(\rho\vec{q}) + \frac{\vec{M}\cdot\bigtriangledown P}{|\bigtriangledown P|} \qquad (4)$$

A shock is then located when this quantity equals or exceeds one.

In the general case, pressure can be related to the internal energy and velocity of the flow with equation 5.

$$p = (\gamma-1)[\rho E - \frac{1}{\rho}(\rho\vec{q})\cdot(\rho\vec{q})] \qquad (5)$$

Taking the time derivative of this quantity will yield the required correction term, equation 6.

$$\begin{aligned}\frac{dp}{dt} &= \frac{(\gamma-1)}{\gamma}[\frac{d}{dt}(\rho H) - \\ &\quad \vec{q}\cdot\frac{d}{dt}(\rho\vec{q}) + \frac{1}{2}q^2\frac{d\rho}{dt}] \qquad (6)\end{aligned}$$

Replacing the time derivatives in equation 6 with their equivalents from the mass and momenum equations yields equation 7.

$$\begin{aligned}\frac{dp}{dt} &= \frac{(\gamma-1)}{\gamma}[-\bigtriangledown\cdot(\rho\vec{q}H) - \\ &\quad \vec{q}\cdot(\bigtriangledown P + \bigtriangledown\rho\vec{q}\vec{q}) - \frac{1}{2}q^2\bigtriangledown\cdot(\rho\vec{q})] \qquad (7)\end{aligned}$$

This is the generalized correction term needed for transient problems.

Translating normal shock in a tube

A model of a moving normal shock in a channel was created to investigate the behavior of the shock finding algorithm and the effect of the transient modification. Two separate runs were done, the first had the initial conditions shown in the figure 8.

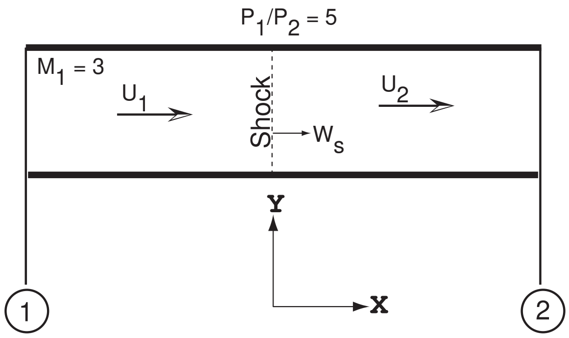

Fig. 8 Transient shock model

Shock relations were used to set up the initial conditions for the model. The formulas for moving normal shock waves with constant C_p and C_v were applicable in this case. However, these formula assume that the upstream speed, U_1 is 0, so a correction had to be made to produce the correct initial conditions for the flow. For the first run, the pressure ratio was chosen to be less than the pressure ratio required for a standing shock in $M = 3$ flow. This required that the shock move toward the right in the positive X direction. The speed of the shock traveling into a stationary fluid, W, was calculated with the equation 8. Since the upstream velocity was not zero, the actual speed of the shock had to be corrected with equation 9.

$$W = a_1\sqrt{\frac{\gamma+1}{2\gamma}(\frac{P_2}{P_1}-1)+1} \qquad (8)$$

$$W_s = U_1 - W \qquad (9)$$

The shock test scalar was calculated with the isentropic transient correction equation (equation 4), that was simplified for this particular example. The Y component of velocity was assumed to be zero in this case, so the divergence term simplified to the following.

$$\frac{1}{|\bigtriangledown P|}\frac{1}{a}\frac{Dp}{Dt} = -a\frac{1}{|\bigtriangledown P|}(\frac{d}{dx}u\rho) + \frac{\vec{M}\cdot\bigtriangledown P}{|\bigtriangledown P|} \qquad (10)$$

The derivative of the density times the X velocity component was then expanded, yielding the final equation.

$$\frac{1}{|\bigtriangledown P|}\frac{1}{a}\frac{Dp}{Dt} = -a\frac{1}{|\bigtriangledown P|}(\frac{du}{dx}\rho + \frac{d\rho}{dx}u) + \frac{\vec{M}\cdot\bigtriangledown P}{|\bigtriangledown P|} \qquad (11)$$

Results indicated that the pressure variation across the shock has some interesting features that are problematic for the shock finding algorithm. The shock started at X=0, and is moving to the right in the positive X direction. As it moves, the shorter wavelengths that makeup the initial discontinuity move at a slower speed than the longer wavelengths. This difference in speed is a numerical artifact of the time stepping method used in the CFD solver. As time progresses, high frequency pressure oscillations show up behind a moving shock, as shown in the figure 9.

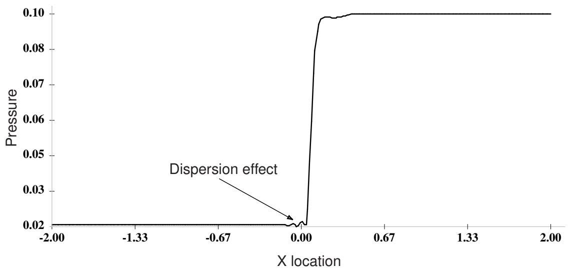

Fig. 9 Pressure distribution

Figure 10 is a plot of the shock scalar with the isentropic transient correction. A filter has been applied to eliminate the pressure gradients caused by dispersion. The dashed line on this and following figures represents the threshold for a shock. Everything above one is marked as a shock region. The value has been plotted at two diferent time values, to show that the shock wave is moving to the right as expected.

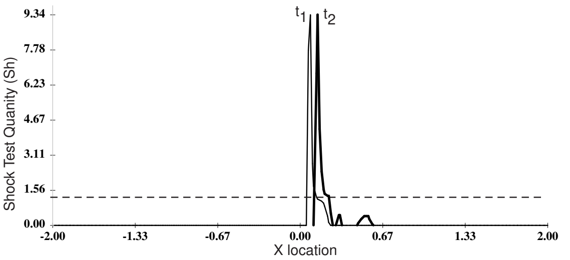

Fig. 10 Shock scalar

The results of this experiment point to the importance of choosing a threshold value for the magnitude of the pressure gradient. Because of the slower wave speeds of the higher frequency pressure waves, oscillations in the pressure gradient take place behind the shock. These pressure gradient increases are enough to skew the results and show up in the shock detection values as a group of shocks behind the actual position as shown in figure 11.

From the above experiment, it was noted that it did not matter if the transient correction was used or not, a shock would still be indicated. This was because the upstream mach number was greater than one, making the uncorrected normal mach number greater than one. A change in initial conditions was made to see what happens when the upstream mach number is

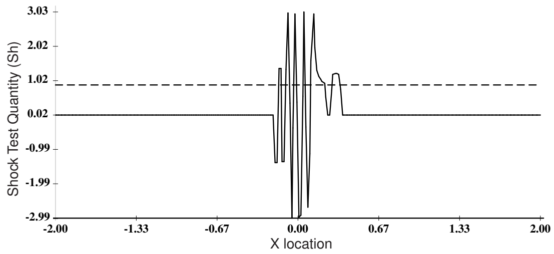

Fig. 11 Shock scalar on unfiltered pressure gradient

less than one. The upstream mach number was set to 0.9,and the pressure difference was set to 3.0, which will produce a normal shock moving in the negative X direction of figure 8.

The results are shown in the following two figures. In the figure 12, the normal mach number is plotted against the x-axis. Notice that the normal mach number does not exceed unity, which by the previous test indicates that no shock is present in the flow. However, the shock test scalar in figure 13 does exceed one at the shock, indicating that the shock is indeed present. The correction term has made it possible to locate the shock.

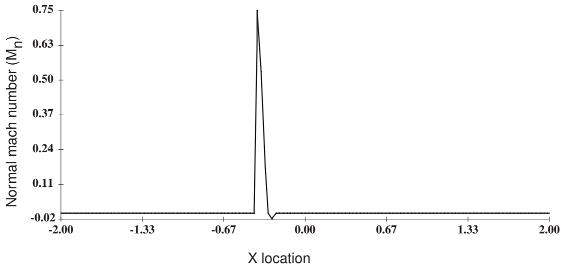

Fig. 12 Normal mach number vs. location

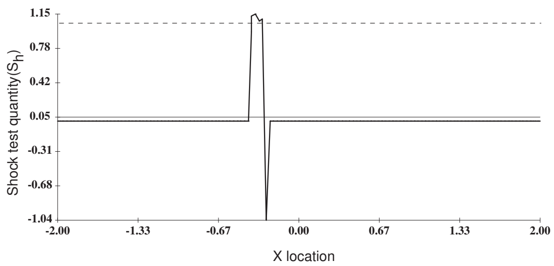

Fig. 13 Shock test variable vs. location

Figure 14 is a plot of the location of maximum in the shock detection value shock vs. time. The figure also contains the shock location, shown in solid lines, calculated by first finding the location of the maximum pressure gradient, and then making a region around this location that is two elements thick. The location of maximum normal mach number is also plotted as a reference. The shock detection maximum lies within three cell widths of the actual shock location, which is acceptable since the numerical scheme used spreads out the shock over three cells.

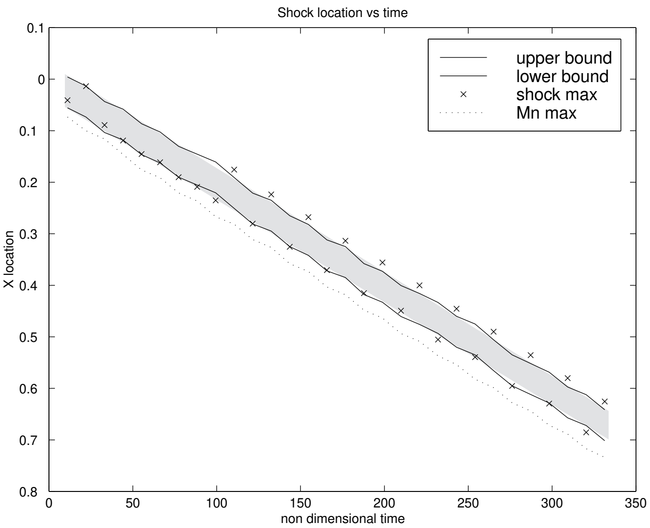

Fig. 14 Theoretical vs. experimental shock location

Filtering

The one dimensional transient results show that this shock finding algorithm produces some falsely indicated shock regions. This is partially due to small numerical errors in the gradient away from the shock. As the magnitude of the pressure gradient goes to zero in the far field, errors in the shock test function become the same order as the indication threshold as shown in the following equation, where δ is a small error in the quantity.

$$\frac{M_n(\bigtriangledown P + \delta \bigtriangledown P)}{|\bigtriangledown P + \delta \bigtriangledown P|} \rightarrow \frac{\delta \bigtriangledown P}{|\delta \bigtriangledown P|} \rightarrow O(1) \qquad (12)$$

To remove these false indications, three filtering techniques have been applied to the problem. The techniques start with an iso-surface constructed where the value of the shock test scalar is 1.0 and reject a subset of the triangles that makeup that surface. The first technique enforces the property that the pressure gradient is normal to the shock surface. This technique removes all shock surface triangles that do not pass the test in the following equation, where n is the normal of the surface triangle, and c is a threshold value between 0 and 1.

$$\frac{|\bigtriangledown P \cdot \vec{n}|}{|\bigtriangledown P|} \leq c \qquad (13)$$

The second technique removes all iso-surface triangles that fall below a certain pressure gradient magnitude threshold. This technique is based on the fact that shock discontinuites should only occur in regions of relatively high gradients. The problem is determining the meaning of a 'relatively' large gradient and setting appropriate threshold. To accomplish this, all the triangles were divided into groups based on the value of the pressure gradient magnitude at their centers. The count of triangles in each group forms a curve. The threshold was chosen where the derivative of this curve goes to zero. This method of setting a threshold assumes that the actual shock surface is located in a region of high gradients and that changing the threshold by some small amount will not change the number of triangles in the surface.

Setting a pressure gradient magnitude threshold can be also be done before the shock iso-surface is constructed by applying the filter to the nodal shock scalar values. If the node does not pass the pressure gradient magnitude test, the shock value can be set to zero. Applying a filter to the nodal values has the advantage of producing a more connected shock surface, without disjoint triangles missing.

A third technique removes all the triangles that do not have jumps in density and temperature that correspond to Rankine-Hugoniot relations. For a moving normal shock, equations 14 and 15 state the relationships between the pressure jump across the shock and density and temperature ratio, respectively.

$$\frac{\rho_2}{\rho_1} = \frac{1 + \frac{\gamma+1}{\gamma-1}\frac{p_2}{p_1}}{\frac{\gamma+1}{\gamma-1} + \frac{p_2}{p_1}} \qquad (14)$$

$$\frac{T_2}{T_1} = \frac{p_2}{p_1}\frac{\frac{\gamma+1}{\gamma-1} + \frac{p_2}{p_1}}{1 + \frac{\gamma+1}{\gamma-1}\frac{p_2}{p_1}} \qquad (15)$$

The difficulty implementing this filtering technique is that the extent of the shock needs to be known before hand, so that the pressure, temperature and density ratios can be accurately measured. To overcome this problem, 20 of measurements of the pressure temperature and density were made on both sides of the surface triangles, then the two measurements that best fit the shock relations were used to determine if the triangle should be rejected. A fitness function was constructed that compares the measured temperature ratio to the temperature ratio computed with equation 15 and the measured density ratio with the computed density ratio of equation 14 and produces a value of 1.0 in the case where the measurements match theory, and less than 1.0 otherwise.

$$f(p_1, p_2, T_1, T_2, \rho_1, \rho_2) \leq 1.0 \qquad (16)$$

If none of the points on either side of the triangle can produce a fitness value of greater than some threshold, the triangle is removed.

To compare the filtering techniques, a measure of difference between the shock test value fields was constructed. The comparison works from a baseline that is assumed to be the actual shock, then the comparison is run against the results of the unfiltered algorithm and the solution with the various types of filtering.

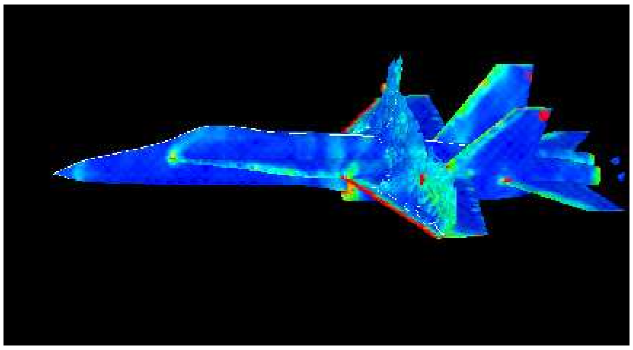

Fig. 15 Stationary shock algorithm on converged solution

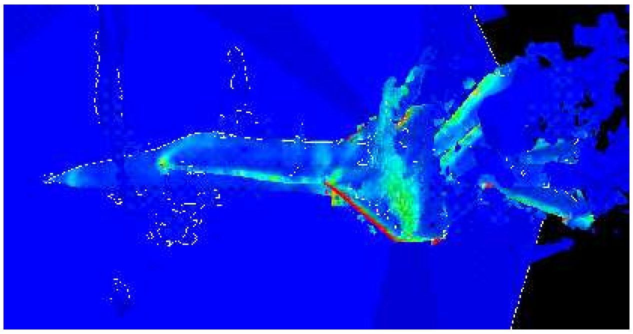

Fig. 16 Transient shock algorithm without filtering

The difference measure is constructed by gathering the centerpoints of all the triangles in the shock surface, F, then all the points that have a shock value greater than 1 in the baseline and test solution are removed from F. The total difference value is the sum of the absolute value of the difference between the values of the baseline and test solution at the points in C as shown in equation 17. The final comparison function takes the total difference and divides it by the final number of triangles in the shock surface.

$$C = F - B \bigcap F \tag{17}$$

Figures 15, 16, and 17 show the results of applying some of the filtering techniques, and why they are necessary. In this case, the solution being examined is an inviscid converged flow on a 300,000 element F18 aircraft model traveling in subsonic flow. Because the solution has run to convergence, the stationary and transient shock finding algorithms should produce the same results, which as figure 16 shows, is not the case. The transient algorithm generates noise and false indications. However, these false signals can be removed with filtering to produce a shock surface that is very similar to the stationary shock finding results. Figure 17 shows the results of running the transient shock finder through a pressure gradient magnitude filter.

Table 2 is a collection of the results from passing the transient shock finder through various combinations of the three filtering algorithms.

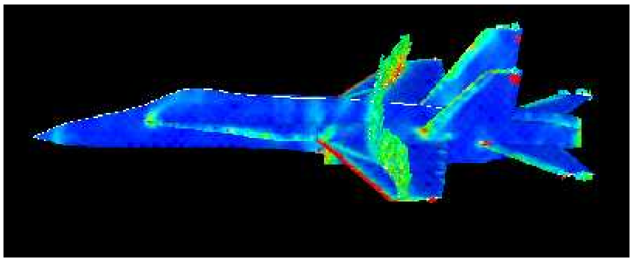

Fig. 17 Transient shock algorithm with pressure gradient magnitude filtering

test case	Comparison function value
no filtering	0.57
$\mid \bigtriangledown P \mid$ filter	0.105
$\mid \bigtriangledown P \mid$ and normal filter	0.223
$\mid \bigtriangledown P \mid$ and jump filter	0.104
jump filter	0.567

Table 2 Filtering study results

The results in table 2 indicate that the pressure gradient magnitude filter alone is better than when used in combination with the other two. This became more evident in looking at the graphical output, where there would be a fairly continuous shock surface at the end of the pressure gradient magnitude filter, with some additional outliers. Applying the normal filter or jump condition filter to these results did not get rid of the outliers, but only removed some of the surface triangles enclosing the shock region, making the final result worse than the result from the pressure gradient magnitude filter alone.

Transonic Aircraft

The transient modifications were tested on a relatively large (1 million element) model of an aircraft traveling in transonic conditions (mach 0.85) to see if the unsteady shock finding algorithm could produce useful results on a realistic model. Figure 18 shows the results of applying the steady state shock finding algorithm to the converged solution. An iso-surface has been constructed where the normal mach number equals one, and this iso-surface is painted with the pressure gradient magnitude as an indication of the shock strength. Note that the thickness of these shock regions is quite small due to the highly refined mesh. Figure 19 is of the same model, but the iso-surface is now plotted on the results from the unsteady shock algorithm.

Since the solution has converged, the unsteady and steady shock results should have been identical. While this was true of the larger shock features, the unsteady algorithm also produced some false indications as in the F18 example. A pressure gradient magnitude filter removed most of this noise, as was necessary in the other examples. However, the shock finder did capture some fairly complex shock structures that would be

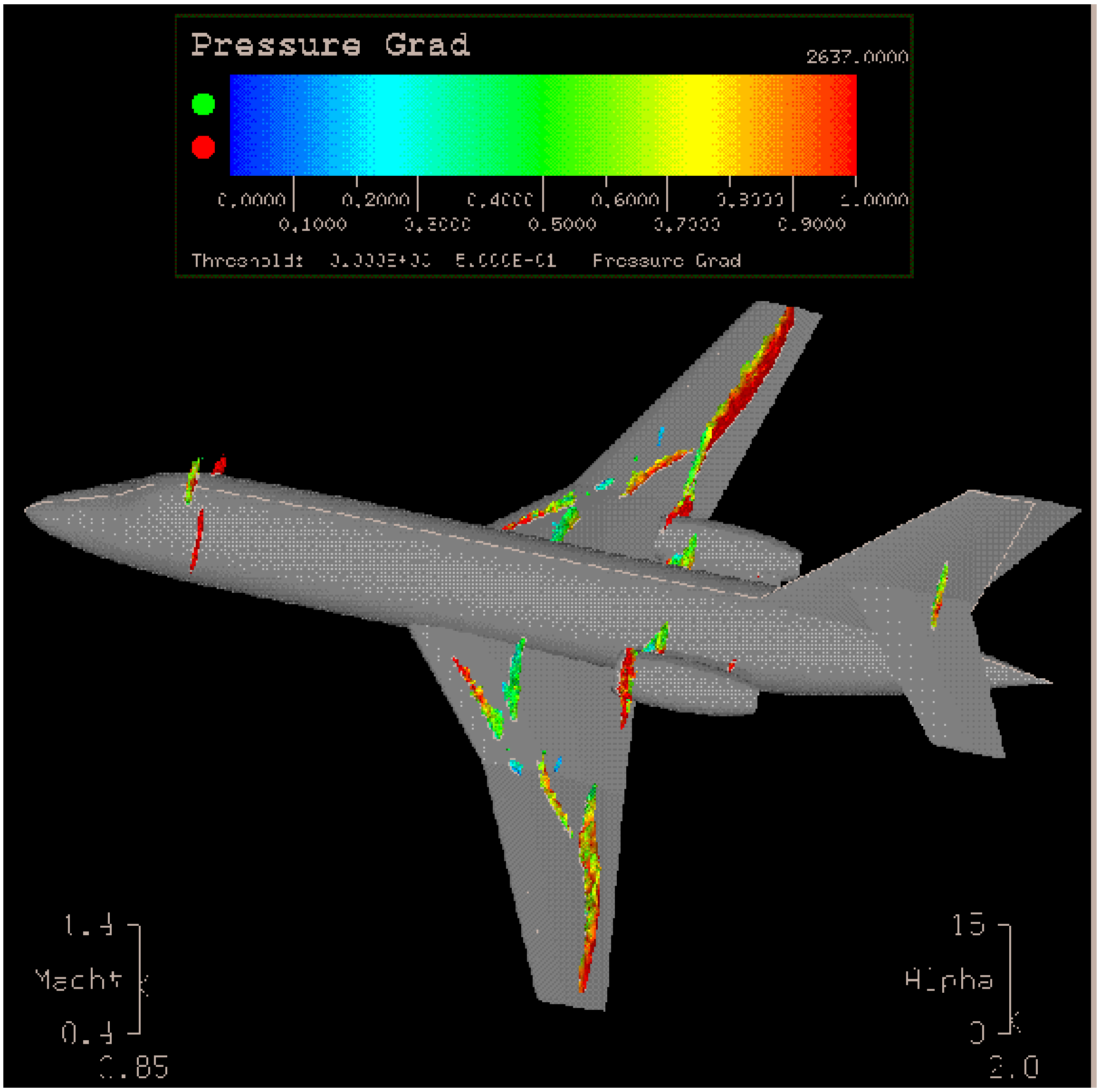

Fig. 18 Steady shock detection results

difficult to find by manually probing the solution field.

Conclusions

The stationary shock finding algorithm developed in this paper does not produce a shock surface that would reflect the shape of the shock in the physical flow, but because of numerical approximation, shows a shock region. The thickness of the region can give information about the quality of the solution and location of needed mesh refinement. Any disperson and dissipation in the solution is reflected in the shape and size of the shock region.

The nature of the solutions and the suceptability of the shock detector to small errors in the solutions makes filtering a requirement, especially in transient solutions. Filtering to enforce jump conditions and shock direction is not as attractive and effective as a simple threshold on the pressure gradient magnitude. The heuristic method of automatically determining this threshold that is presented in this paper was effective on the models tested.

Shock finding based on fluid dynamic principles is practical, with some advantages over more general edge detection, but requires filtering of the results.

Acknowledgments

This has been an extension of the work done by David Darmofal[3] and professor Mark Drela was instrumental in finding the unsteady extensions to the basic algorithm. I would also like to thank Ravi Samtaney at NASA Ames for sharing his ideas about filtering algorithms.

Funding for this project has been provided by NASA Ames, through grant number NCC2-985, and by the Army under grant DAAG55-97-1-0394. Additional support for this research was obtained from the IBM SUR Project and the IBM UUP Project.

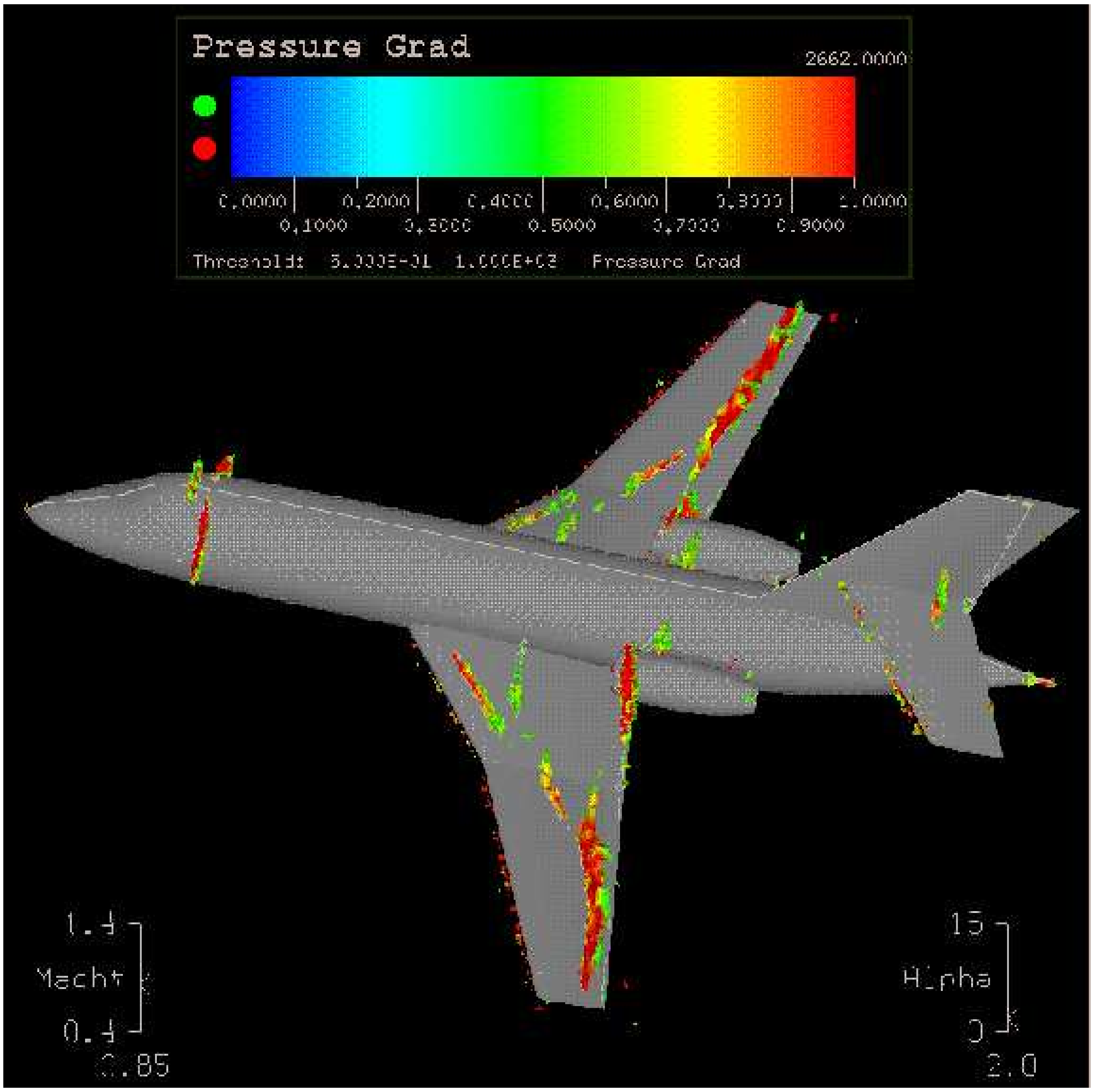

Fig. 19 Unsteady shock detection results

References

[1]Kwan-Liu, Ma Van Rosendale, John Vermeer, Villem "3D Shock Wave Visualization on Unstructured Grids"

[2]Anderson, John D Jr.,"Modern Compressible Flow with Historical Perspective" McGraw-Hill, 1982

[3]Darmofal, David,"Hierarchal Visualization of Three-Dimensional Vortical Flow Calculations" MIT 1991

[4]Pagendarm, H-G B. Seitz: in P Palamidese(ed.):"Visualization in Scientific Computing" Ellis Horwood Workshop Series, 1993

[5]Walatka, P.P. Burning, P.G. Elson, Pierce L.,"Plot3D Users Manual, NASA TM 101067" July 1992

[6]L. Hesselink, Y. Levy, Rajesh Batra,"Automatic Flow Feature Extraction for use in Computational Steering of Aerodynamic Design Processes" http://www-leland.stanford.edu/ rbatra/ics/ics.html

[7]Liepmann, H. W. Roshko A.,"Elements of Gasdynamics" John Wiley&Sons, 1957